Journal of Power Sources 185 (2008) 1557–1562

Contents lists available at ScienceDirect

Journal of Power Sources

journal homepage: www.elsevier.com/locate/jpowsour

A competitive candidate material for aqueous supercapacitors: High surface-area graphite

Hui-Qiao Li, Yong-Gang Wang, Cong-Xiao Wang, Yong-Yao Xia *

Department of Chemistry and Shanghai Key Laboratory of Molecular Catalysis and Innovative Materials, Fudan University, Shanghai 200433, China

ARTICLE INFO

Article history:
Received 2 July 2008
Received in revised form 24 August 2008
Accepted 27 August 2008
Available online 3 September 2008

Keywords:
Graphite
Activated carbon
Supercapacitors
Ball-milling

ABSTRACT

The specific surface area of flake natural graphite can be definitely increased from 7 $m^2 g^{-1}$ to 580 $m^2 g^{-1}$ by high-energy ball-milling. The obtained high surface-area graphite (HSG) was first investigated in detail as a new kind of electrode material for aqueous supercapacitors. HSG sample obtained by long-time ball-milling showed quite large capacitance, e.g. 205 F g^{-1} for 70 h milling. The high capacitance of HSG might profit from the high open surface area contributed by the nanoparticle exterior, the large quantity of lattice defects, as well as the high density of oxygen functional groups in HSG produced by high-energy ball-milling. The capacitance of HSG maintained well during 5000 cycles of charge/discharge process. Moreover, compared to the commercial activated carbon which has a fully developed porous structure, HSG promised a high electrode density due to its low porosity thus it exhibited a much higher volumetric capacitance than commercial activated carbon.

1. Introduction

The energy stored in electrochemical double layer capacitors (EDLCs or supercapacitors) derives from the separation of charged species in the electric double layer across the electrode/electrolyte interface, so the commercialized EDLCs have been studied exclusively on activated carbon (AC) materials due to their ultrahigh surface area per unit weight (even up to 3000 $m^2 g^{-1}$). However, the proportionality between the capacitance and specific surface area of ACs is not observed especially in the case of high current density because the large quantity of micropores (<2 nm) in AC cannot be easily accessible for electrolyte [1,2] thus will not contribute to the total capacitance of the materials. In recent years, highly ordered mesoporous carbons (OMCs) were successfully synthesized by nano-casting approaches in which mesoporous silicas were used as the hard templates [3]. Attribute to the uniform mesopore channels, OMC promised higher surface efficiency and better rate capability than AC, but with a lower specific capacitance due to its lower surface area (1200–1500 $m^2 g^{-1}$) [4–6]. In addition, the extra step to prepare the silica scaffolds made the industrial application of OMCs more difficult.

Since capacitance depends strongly on the electrolyte accessible surface of the electrode material, it is easy to be recognized that the porous structure for AC and OMC is originally developed to solely increase the effective reaction area. However, a highly porous structure leads to not only a low electrode density but also a relative low surface efficiency since a great part of the pore surface specially contributed by micropores, closed-pores etc., cannot be effectively utilized in EDLC. By turning, it would be most advantageous if an electrode material was designed of large surface area with an open pore structure or low porosity, for example, a high surface electrode material which consists of numerous nanosized sheets. It was reported that the specific capacitance of graphite for edge plane was 50–70 μF cm^{-2} [7], much higher than that of other carbonaceous materials, e.g. 7–10 μF cm^{-2} for AC and OMC [6,8]. Mechanical grinding has been proved an effective way to increase the total surface area of graphite; however, the obtained high surface-area graphite (HSG) was mainly studied as a lithium storage material [9–13]. Some researchers investigated the possibility of ball-milled graphite in EDLC but only focused on its specific capacitance in non-aqueous electrolyte [9,14]. Little attention has been made to other important factors for EDLC application, such as rate capability, cycle life, and electrode density etc. On the other hand, all the mechanical grinding were carried out under specific atmosphere, e.g. H_2, Ar, O_2, which inevitably gave rise to some H or O impurity in the graphite sample [9,15,16]. These hetero-elements might disturb the ingress of ions to the micropores of the carbon and sometimes lead to deterioration by electrolysis especially in non-aqueous electrolyte [17,18]. In this paper, we for the first time investigated the detailed capacitive behaviors of a kind of HSG in aqueous solution. HSG was prepared by high-energy ball-milling under air atmosphere with flake natural graphite as the start mate-

* Corresponding author. Fax: +86 21 55664177.
E-mail address: yyxia@fudan.edu.cn (Y.-Y. Xia).

0378-7753/$ – see front matter © 2008 Published by Elsevier B.V.
doi:10.1016/j.jpowsour.2008.08.079

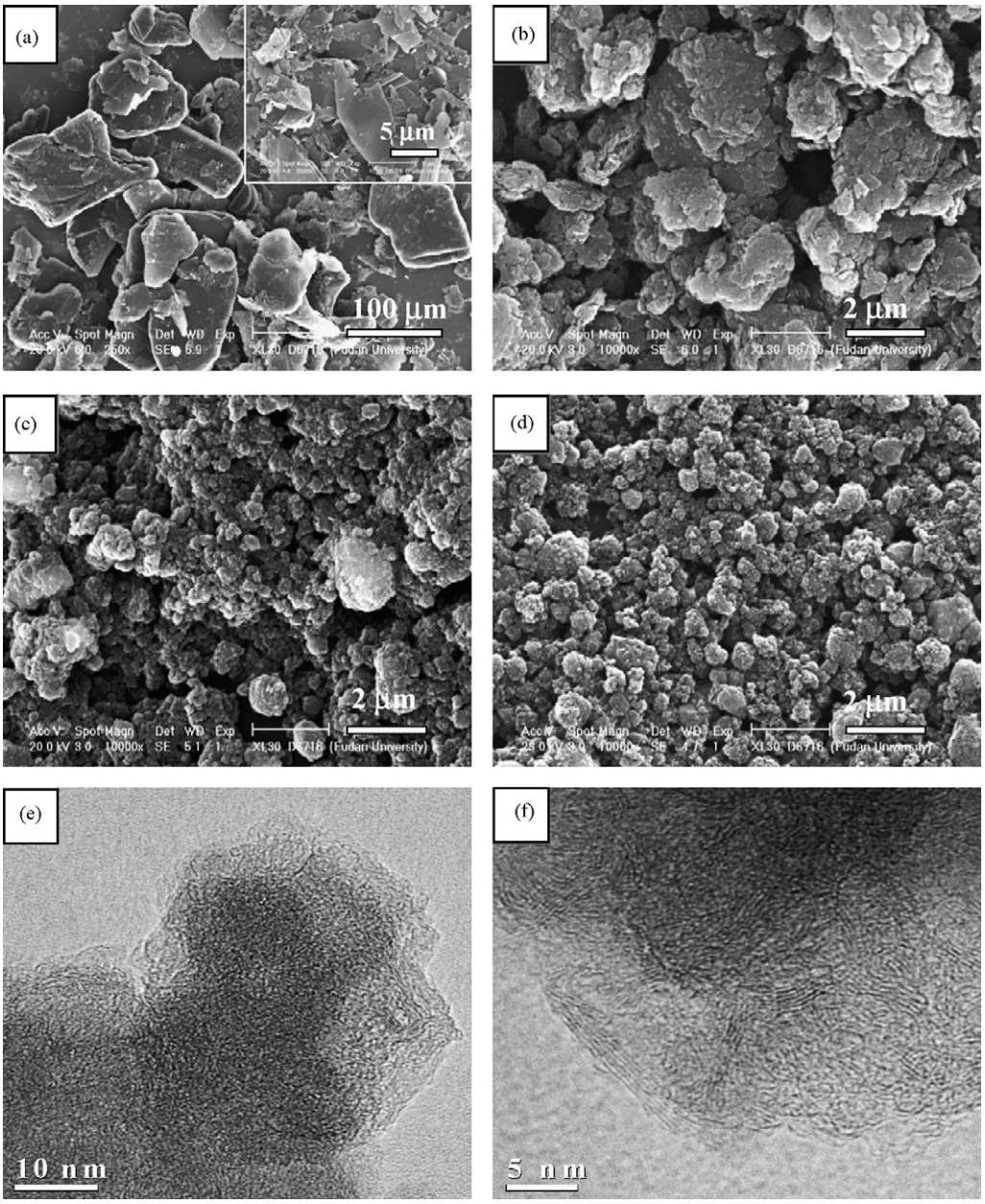

Fig. 1. SEM graphs of HSG obtained by milling for 0 h (a), 5 h (b), 20 h (c), and 50 h (d). (e and f) TEM graphs of HSG obtained by milling for 50 h.

rial. Although the electrochemical results show that a good balance should be made between the specific capacitance and rate capability, HSG still promised quite competitive performances compared with commercial AC especially in view of volumetric energy density.

2. Experimental

2.1. Synthesis of HSG

20 g of commercial high-purity flake natural graphite powder and 30 stainless steel balls (10 mm in diameter, 3.8 g) were introduced into a stainless steel jar (50 mL in volume) mounted on a high-energy planetary mono mill pulverisette 6 (Fritsch GmbH. Inc., Germany). The ball-milling treatments were performed with a rotatory speed of 400 rpm at room temperature (~25 °C) under air atmosphere. To avoid the increase in temperature during milling process, the milling treatment was interrupted every 30 min and rested for 30 min. The samples collected after milling were named as HSG-*X* in which *X* denoted the corresponding milling time (h).

2.2. Characterization of HSG

The morphologies of the HSG-*X* samples were characterized with scanning electro microscopy (SEM) conducted on a Philips XL-60 scanning microscope. The X-ray diffraction (XRD) patterns of these samples were recorded by a Bruker Advance 8 X-ray diffractometer with Cu Kα radiation. Raman measurements were taken by a Dilor Labram-1B spectrograph. Nitrogen sorption isotherms were measured at 77 K with a Micromeritics Tristar 3000 analyzer (USA). Before measurements, the samples were degassed in vacuum at 200 °C for at least 6 h. Brunauer–Emmett–Teller (BET) method was used to analyze the specific surface area of the samples. The ele-

mental analysis was conducted on Vario EL III elemental analysis instrument.

2.3. Electrochemical measurements

The electrode was prepared by mixing of 95 wt.% HSG powder and 5 wt.% poly(tetrafluoroethylene) (PTFE) binder dispersed in isopropanol. The resulting slurry was pressed onto the Ni foam current collector and then dried at 120 °C for 12 h to remove the solvent and water. The typical mass load of the electrode was 5 mg cm^{-2}. The electrochemical behaviors of HSG were characterized by cyclic voltammetry (CV) and galvanostatic charge/discharge measurements using a three-electrode glass cell in which Pt foil was used as the counter electrode, Hg/HgO electrode was used as the reference electrode and 6 M KOH solution was used as the electrolyte. All the electrochemical measurements were performed using a Solartron Instrument Model 1287 electrochemical interface controlled by a computer. For comparison, the commercial AC (Mitsubishi, Japan) electrode was also prepared by the same procedure as described above. The BET surface of the commercial AC was 2100 m^2 g^{-1}, the total pore volume was 1.12 cm^3 g^{-1}, and the particle size was about 5–10 μm.

3. Results and discussion

3.1. Morphology of HSG

The SEM graphs of HSG samples showed the morphology evolution in the process of high-energy ball-milling. The large grains of the start material NG (HSG-0) ranged from 10 μm to 20 μm in size and showed typical flake morphology within the grains as observed by the inset image of Fig. 1a. As seen in Fig. 1b, the grain size was reduced to 1/10 after 5 h ball-milling, together with the fragmentation of the large flakes. The scrunched flakes began to pile up to small particles. For HSG-20 in Fig. 1c, the original large grains of natural graphite were completely crushed into random particles whose size was much smaller than HSG-5. These nanosized particles were not stable thus agglomerated into sub-particles to reduce the high surface energy. With longer milling time, e.g. HSG-50 in Fig. 1d, it showed more seriously agglomeration of nanoparticles due to the increasing surface energy when the particle size is decreasing. More detailed morphology of these nanoparticles can be observed by the TEM graphs of HSG-50. The mean diameter of the nanoparticles was about 20–30 nm according to Fig. 1e, and within the nanoparticle, it was composed of many misoriented basic structure units (BSU, conjugated benzene-ring like planes). It is known that NG has a perfect stacking order of well-crystalline layers in the *c*-direction. The observation obviously demonstrated that the infinite stacking layers of pristine NG had been intensely exfoliated and fractured into small pieces of BSU after long-time ball-milling, indicating that the energy generated by mechanical milling was high enough to break the covalent bond within the graphene planes. Seen from Fig. 1f, the random distribution of BSU domains led to a high ratio of disorder, however, many BSU domains still consisted of three to five layers of ordered stacking graphene planes. This considerable remaining of graphite microcrystallites would be in favor of a good conductivity when applied as an electrode material.

3.2. Structural evolution of HSG

The XRD patterns for HSG-5, HSG-20 and HSG-50 were shown in Fig. 2. Three broad diffraction peaks were observed near 26°, 43° and 78°, which correspond to (0 0 2), (1 0 0) and (1 1 0) reflections, respectively. A sharp decrease in intensity as well as a broadening of the (0 0 2) Bragg peak can be observed along with the increase

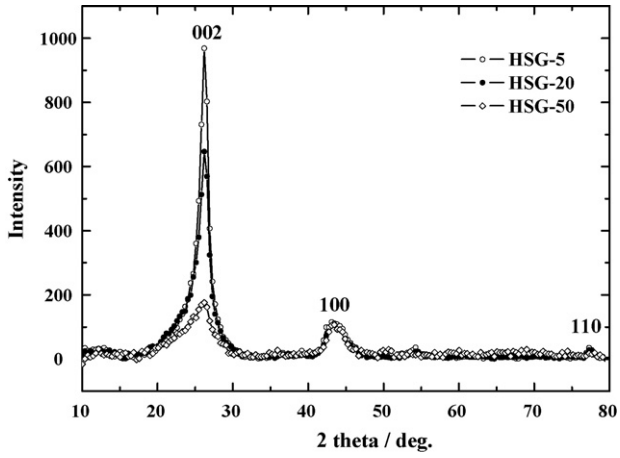

Fig. 2. XRD patterns of HSG samples obtained at milling time of 5, 20, and 50 h.

of milling time. The size of the graphite microcrystallite in *c*-axis direction, i.e. *Lc* (parallel to the edge plane), can be determined using the XRD patterns from Scherrer's equation given by the following equation:

$$L = \frac{k\lambda}{B\cos\theta}$$

where *L* is the microcrystallite size, *k* is the Scherrer parameter (*k* = 0.89 for *Lc*), λ is the wavelength of X-ray beam, *B* is the angular width of the diffraction peak at half maximum intensity and θ represents the Bragg angle [19]. The broadening of (0 0 2) peak indicated *Lc* decreased with the increase of milling time, which deduced the exfoliation process of graphene layers. The calculated *Lc* for HSG-50 was about 1.1 nm, comparable to an average thick of three stacked graphene layers. Furthermore, the low intensity of (0 0 2) peak suggested many defects, such as vacancies, vacancy line and loops, were also induced by mechanical milling [20]. These lattice defects in HSG broke down the hexagonal symmetry of the graphite lattice thus result in much lower diffraction intensity than that of NG whose intensity of (0 0 2) peak was over 20,000 at the same condition of detecting.

The Raman spectra of four HSG samples obtained at different milling time were shown in Fig. 3. All the samples exhibited two Raman bands at 1580 cm^{-1} (namely G band), which corresponds to the E_{2g} vibration (C=C aromatic; C sp^2) and 1350 cm^{-1} (namely D band). The D and G bands are usually assigned to the bands of

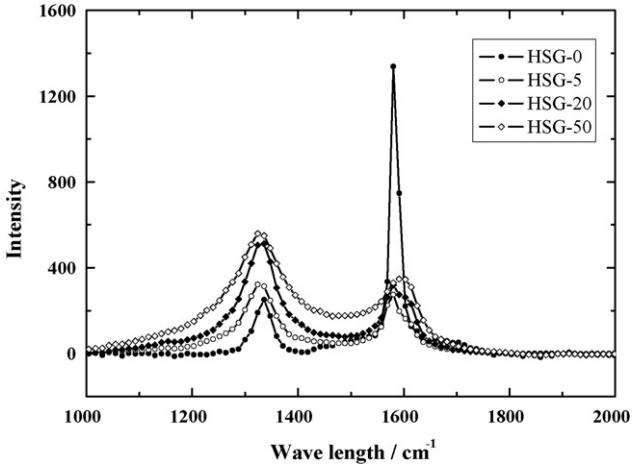

Fig. 3. Raman spectra of HSG samples obtained by milling for 0, 5, 20, and 50 h.

graphitized carbon and disordered carbon, respectively. The relative intensity (I_D/I_G), where I_D is the area of the D band and I_G is the area of the G band, has been used to determine the graphitization degree of carbon species. The large quantity of lattice defects which increased with the prolonged milling time modified the optical selection rules for the lattice vibration modes thus led to a rapid increase of D band. The I_D/I_G of HSG-0, HSG-5, HSG-20 and HSG-50 was estimated to be about 0.01, 1.17, 1.51, 1.71, respectively, indicating an increased ratio of disorder in HSG as confirmed by TEM and XRD observation above.

3.3. Electrochemical properties of HSG

Specific surface area is the primary key factor of double layer capacitance. The time dependences of BET surface area and specific capacitance were shown in Fig. 4. In the initial 20 h milling, the BET surface area drastically increased from 7 $m^2\,g^{-1}$ (for NG) to a maximum value of 580 $m^2\,g^{-1}$ (for HSG-20) upon the increase of milling time; after that, the surface area decreased slowly with the milling time. The two distinctive steps of BET surface area were similar to the behavior of graphite grounded by shock-type interaction which experienced three successive stages of division–fracture–agglomeration [12]. The surface area increased at the initial milling hours due to the exfoliation of graphene layers as well as the decrease of particle size. Then the mechanical energy cumulated by long-time milling would produce a high density of defects into the exfoliated graphene layers, which consequently resulted in their fracture. The so-obtained fresh fragments were not stable that they would be stabilized by means of agglomeration, hence, the specific surface area decreased. However, the corresponding specific capacitance for HSG demonstrated a different tendency from their BET surface upon the milling time. CV measurements using a three-electrode system were conducted from 0.05 V to −0.85 V vs. Hg/HgO in 6 M KOH solution. And the differential capacitance, calculated by $dC = i/\nu$ in which i is the average current density ($A\,g^{-1}$) at −0.4 V vs. Hg/HgO, ν is the scan rate (here used 10 $mV\,s^{-1}$), was chosen to estimate the specific capacitance for each HSG sample. As seen in Fig. 4, the capacitance underwent a fast growth at the first stage and then a relatively slow growth at long milling time. HSG-0 (NG) with a much low specific surface area of 7 $m^2\,g^{-1}$ showed nearly no capacitance. HSG-20 with the highest surface area of 580 $m^2\,g^{-1}$ showed a capacitance of 150 $F\,g^{-1}$, while HSG-70 with a surface area of 313 $m^2\,g^{-1}$ showed the highest specific capacitance of 205 $F\,g^{-1}$. The abnormality between the surface area and capacitance might be attributed to the cumulative effects of high surface, lattice defects, and surface oxygen functional groups. First, long-time milling would increase the density of lattice defects which cause the fracture of graphite layers. The fracture of graphite layers led to an increased ratio of basal to edge carbon surface as well as C-dangling bonds. The specific capacitance of graphite was reported to be 3 and 50–70 $\mu F\,cm^{-2}$ for its basal plane

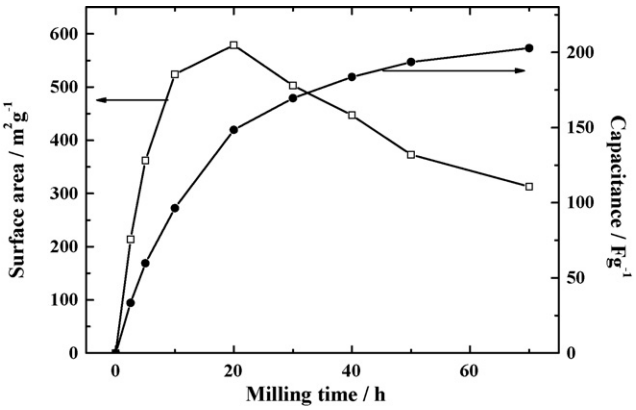

Fig. 4. Evolution of the BET surface area and the capacitance for HSG as a function of milling time, the capacitance was calculated by the CV measurement of 10 $mV\,s^{-1}$ at −0.4 V vs. Hg/HgO according to $dC = i/\nu$.

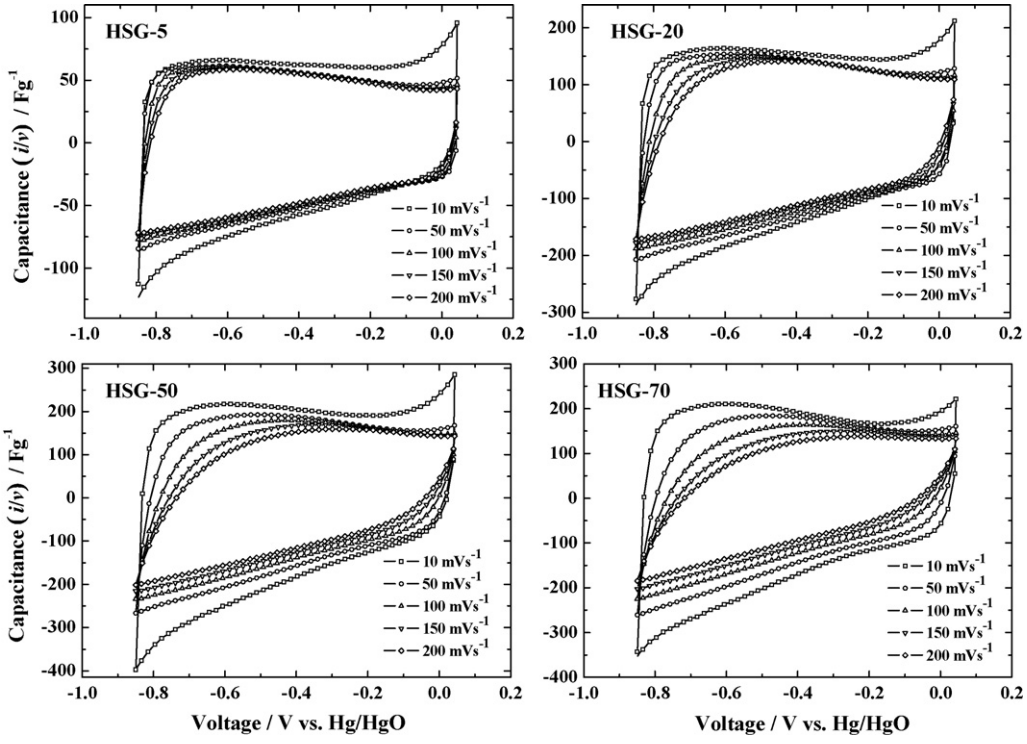

Fig. 5. Voltammograms of HSG-5, HSG-20, HSG-50 and HSG-70 at different scan rates of 10–200 $mV\,s^{-1}$ between 0.05 V and −0.85 V vs. Hg/HgO in 6 M KOH solution.

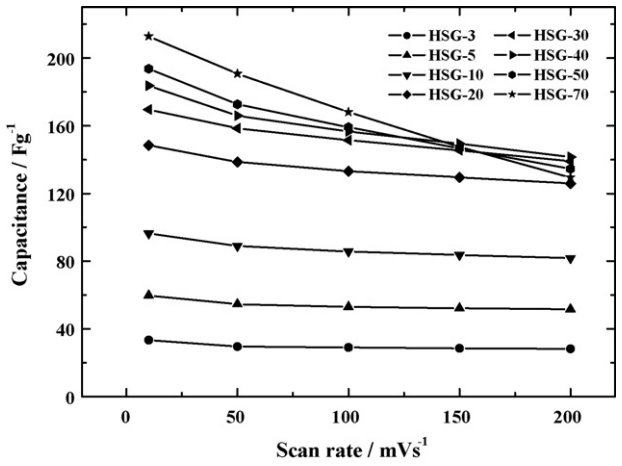

Fig. 6. Comparison of capacitance decay with increasing scan rates for HSG samples obtained by milling for different hours.

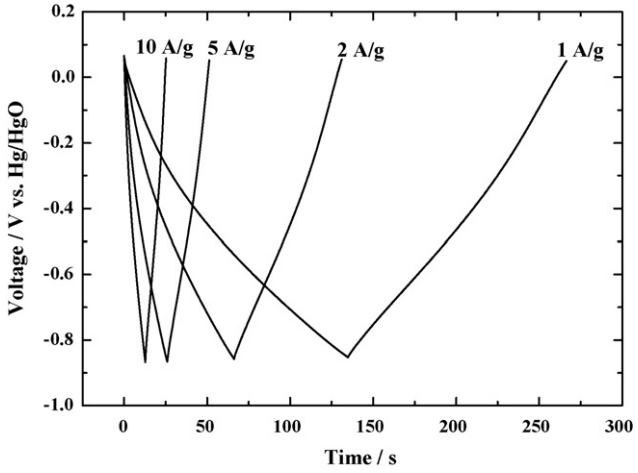

Fig. 7. Galvanostatic charge/discharge curves of HSG-30 between 0.05 V and −0.85 V vs. Hg/HgO at different current densities.

and edge plane, respectively [7]. The oxygen functional group was another important factor. The oxygen in the atmosphere would participate in the agglomeration of the exfoliated and broken graphene layers by forming C—O—C bridges with the C-dangling bonds at the boundaries of the carbon edges. Longer time milling gave rise to higher density of O-functional group. According to the elemental analysis in which we assumed the oxygen wt.% = 100% − C% − H%. The oxygen weight percentage was estimated to be 14%, and 10% for HSG-70 and HSG-30, respectively. The oxygen weight of ball-milled graphite under pure O_2 atmosphere for 20 h milling was reported by Chevallier et al. [9] to be about 8%. The contribution of pseudo-capacitance might grow with the milling time thus HSG-70 showed the highest capacitance.

Fig. 5 presented the voltammograms of HSG-10, HSG-20, HSG-50, HSG-70 at different scan rates varying from 5 mV s^{-1} to 200 mV s^{-1} between 0.05 V and −0.85 V vs. Hg/HgO in 6 M KOH solution. At low scan rates, all the samples showed quite rectangular curve shape without observation of obvious oxygen and hydrogen evolution peaks, suggesting a typical nonfaradic adsorption/desorption reaction in this window. It is well known that the voltammogram shape is affected by the RC time constant (τ) of the electrode. A larger τ results in a longer transient part (less steepness in the current change of CV curve at the switching potential), which means worse collapse of the rectangular shape. The voltammograms of HSG-10 maintained a very good box-like shape at all scan rates; while HSG-20 showed an acceptable retention of rectangular shape at elevated scan rates. The nearly 90° change in the CV curves of HSG-10 and HSG-20 at the switching potential suggested that they had small time constants as an ideal capacitor desired, which can be attributed to their good conductivity inherited from the graphite nanocrystallites. As for HSG-50 and HSG-70, the distortion of CV curves at high scan rates became more and more serious, corresponding to an increasing τ. The enhanced distortion of CV profiles can be explained by the deteriorated conductivity of HSG due to the more intense destruction of graphite structure by much longer time milling.

The affection of milling time to the rate capability of HSG can be more clearly observed by Fig. 6 in which the capacitances at different scan rates were presented. HSG samples with milling time within 30 h maintained their capacitances very well even at large scan rates up to 200 mV s^{-1}. Above 40 h, the capacitances began to decay in an accelerated speed in the sequence of HSG-40, HSG-50, HSG-70. The deteriorated capacitive performances upon milling time suggested a good balance should be made between the specific capacitance and the rate capability of HSG when used as an EDLC electrode material. Therefore, we chose a sample obtained at a medium milling time for the further investigation.

The galvanostatic charge/discharge curves of HSG-30 (502 m^2 g^{-1}) at different current densities were shown in Fig. 7. It exhibited typical triangle-shaped curves between 0.05 V and −0.85 V vs. Hg/HgO with a good inverse proportion between the discharge time and the employed current density. Even at a current density of 10 A g^{-1}, there was no observation of obvious voltage drop at the current switches, indicating a quite low resistance of the electrode. The capacitances of HSG-30 obtained at different current densities were shown by Fig. 8 in comparison with commercial AC (2100 m^2 g^{-1}). When the current density was lower than 1 A g^{-1}, both HSG-30 and AC showed a considerable capacitance loss due to the concomitant gas evolution reaction which was more appreciable at low current. When the current density was increased from 1 A g^{-1} to 10 A g^{-1}, the capacitance of HSG-30 remained well in about 170 F g^{-1}, showing an excellent rate capability. A similar tendency of capacitance was observed for AC but with a slight higher specific capacitance of 182 F g^{-1}. Taking the specific surface area into account, the specific capacitances of HSG-30 and AC were estimated to be 33 and 8.6 μF cm^{-2}, respectively. The large specific capacitance of HSG-30 might be contributed by both the large amount of edge planes produced by high-energy ball-milling and the rough basal planes containing many crystal defects.

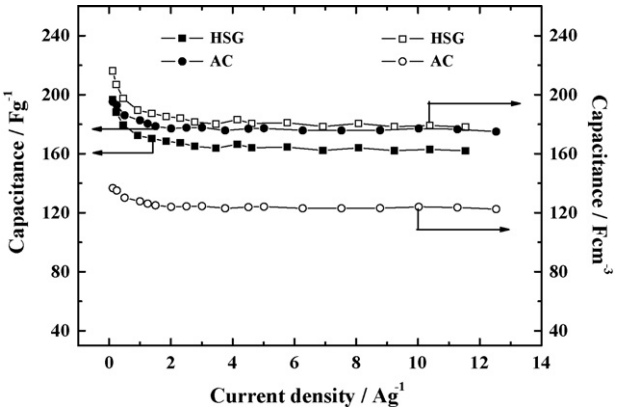

Fig. 8. Gravimetric and volumetric specific capacitances of HSG-30 and AC upon the increase of current loading.

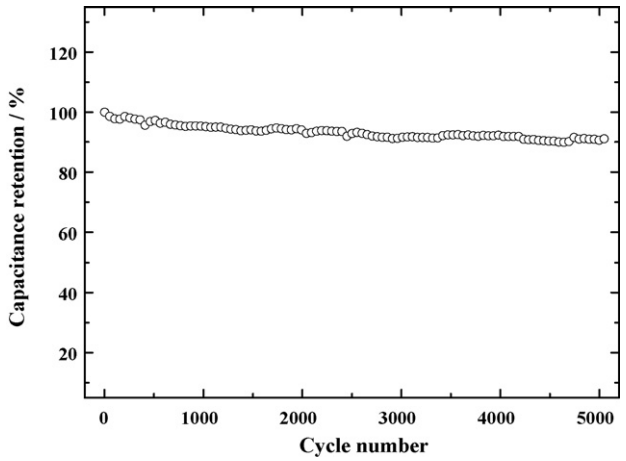

Fig. 9. Capacitance retention of HSG-30 during 5000 cycles of charge/discharge between 0.05 V and −0.85 V vs. Hg/HgO.

The micromation of industrial products requires power sources of high volumetric energy. The trade-off between the porosity and the stack density makes it quite difficult for porous AC to achieve a high electrode density when referred to assembling an EDLC. Profit from the low porosity, HSG promised a high electrode density of 1.0 mg cm^{-3}, in comparison with a quite lower electrode density of 0.7 mg cm^{-3} for commercial AC. Therefore, HSG-30 showed a much higher volumetric energy density than AC. As seen in Fig. 8, the volumetric specific capacitance of HSG-30 was about 180 F cm^{-3} at 10 A g^{-1}, nearly 1.5 times of that for AC (about 120 F cm^{-3}).

The stability of HSG-30 was also investigated by galvanostatic charge/discharge at a current density of 1 A g^{-1} from −0.05 V to −0.85 V vs. Hg/HgO. As shown in Fig. 9, it maintained over 90% of the initial capacitance after 5000 cycles of charge/discharge. The good cycle performance of HSG-30 indicated that a stable energy storage process was repeated during the long cycle charge/discharge process. All the above results demonstrated that HSG could be considered to be an excellent EDLC electrode material.

4. Conclusion

A new kind of electrode material called high surface-area graphite was developed for EDLC. The highly ordered graphene layers of natural graphite was intensely exploited and then broke into nanosized fractures by high-energy ball-milling thus resulted in a remarkable increase of surface area, a high density of lattice defects, as well as the high density of oxygen functional groups. The BET surface area of HSG experienced a rapid increase and then a decrease upon the milling time due to a successive division–fracture–agglomeration process during ball-milling. Long-time milling led to an increased capacitance for HSG but in the same time with deteriorated conductivity. HSG sample obtained at a medium milling time showed a large specific capacitance of 33 μF cm^{-2} and a good cycle performance during 5000 cycles of charge/discharge. Attribute to the remaining of graphite nanocrystallites, HSG electrode showed a good rate capability at high current densities. More important, the low porosity of HSG favored a higher electrode density than the conventional porous carbons such as AC and OMC, thus promised a high volumetric energy density. The results demonstrate that HSG is a hopeful EDLC material for practical application especially in consideration of the cost.

Acknowledgements

This work was partially supported by the National Natural Science Foundation of China (No. 20633040), State Key Basic Research Program of PRC (2007CB209700), and the 863 Program of China (No. 2006AA05Z218).

References

[1] E. Frackowiak, F. Beguin, Carbon 39 (2001) 937.
[2] D. Du, H. Shi, J. Power Sources 74 (1998) 99.
[3] S. Jun, S.H. Joo, R. Ryoo, M. Kruk, M. Jaroniec, Z. Liu, T. Ohsuna, O. Terasaki, J. Am. Chem. Soc. 122 (2000) 10712.
[4] S. Yoon, J. Lee, T. Hyeon, S.M. Oh, J. Electrochem. Soc. 147 (2000) 2507.
[5] S. Alvarez, M.C. Blanco-Lopez, A.J. Miranda-Ordieres, A.B. Fuertes, T.A. Centeno, Carbon 43 (2005) 866.
[6] W. Xing, S.Z. Qiao, R.G. Ding, F. Li, G.Q. Lu, Z.F. Yan, H.M. Cheng, Carbon 44 (2006) 216.
[7] J. Randin, E. Yeager, J. Electroanal. Soc. 118 (1971) 711.
[8] H.S. Zhou, S.M. Zhu, M. Hibino, I. Honma, J. Power Sources 122 (2003) 219.
[9] F. Chevallier, L. Aymard, J.M. Tarascon, J. Electrochem. Soc. 148 (2001) A1216.
[10] F. Disma, L. Aymard, L. Dupont, J.M. Tarascon, J. Electrochem. Soc. 143 (1996) 3959.
[11] F. SalverDisma, C. Lenain, B. Beaudoin, L. Aymard, J.M. Tarascon, Solid State Ionics 98 (1997) 145.
[12] F. Salver-Disma, A. Du Pasquier, J.M. Tarascon, J.C. Lassegues, J.N. Rouzaud, J. Power Sources 82 (1999) 291.
[13] R. Alcantara, P. Lavela, G.F. Ortiz, J.L. Tirado, R. Menendez, R. Santamaria, J.M. Jimenez-Mateos, Carbon 41 (2003) 3003.
[14] E. Gomibuchi, T. Ichikawa, K. Kimura, S. Isobe, K. Nabeta, H. Fujii, Carbon 44 (2006) 983.
[15] T.S. Ong, H. Yang, Carbon 38 (2000) 2077.
[16] M. Francke, H. Hermann, R. Wenzel, G. Seifert, K. Wetzig, Carbon 43 (2005) 1204.
[17] Y.J. Kim, Y. Horie, S. Ozaki, Y. Matsuzawa, H. Suezaki, C. Kim, N. Miyashita, M. Endo, Carbon 42 (2004) 1491.
[18] D. Lozano-Castello, D. Cazorla-Amoros, A. Linares-Solano, S. Shiraishi, H. Kurihara, A. Oya, Carbon 41 (2003) 1765.
[19] G.J. Lee, S.I. Pyun, Electrochim. Acta 51 (2006) 3029.
[20] C.S. Wang, G.T. Wu, W.Z. Li, J. Power Sources 76 (1998) 1.